Supplementary information

High-entropy nanoparticles constructed porous honeycomb as a 3D sulfur host for lithium polysulfide adsorption and catalyzing in Li-S batteries

Zhiyu Zhou[abc], Zexiang Chen*[abc], Huifang Lv[abc], Yang Zhao[abc], Hualiang Wei[abc], Guoli Huai[a], Ruxiang Xu*[a], and Yan Wang*[abc]

[a]Sichuan Provincial People's Hospital, University of Electronic Science and Technology of China, Chengdu, China

[b]School of Optoelectronic Science and Engineering, University of Electronic Science and Technology of China, 611731 Chengdu, China

[c]Sichuan Province Key Laboratory of Display Science and Technology, Jianshe North Road 4, 610054 Chengdu, China

E-mail: zxchen@uestc.edu.cn (Zexiang Chen); xuruxiang1123@uestc.edu.cn (Ruxiang Xu); wangyan127@uestc.edu.cn (Yan Wang)

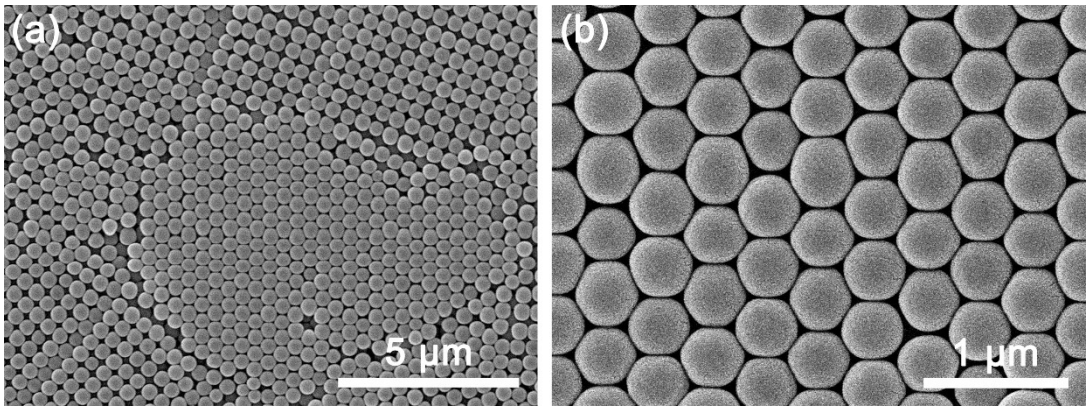

Fig. S1. The PS spheres used for the synthesis of the MgCrMnFeCoNi-O honeycomb.

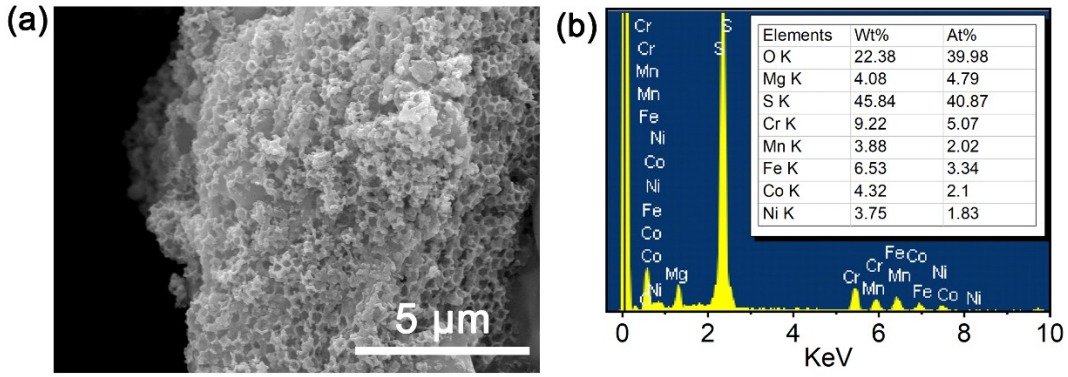

Fig. S2. (a) Morphology of the sulfur-loaded MgCrMnFeCoNi-O honeycomb and (b) corresponding EDS analysis.

Fig. S2 displays an SEM image and corresponding EDS analysis of the prepared sulfur-loaded MgCrMnFeCoNi-O cathode. In Fig. S2a, the resultant sulfur/MgCrMnFeCoNi-O composite exhibits apparent differences in morphology compared with the pristine MgCrMnFeCoNi-O host (Fig. 2b-2d). It can be found that the sublimed sulfur solids infused into the pores and filled the interior space of the MgCrMnFeCoNi-O. This is because sulfur powders melted into liquid under 155 ^{o}C and flowed into the porous HEA host in the synthesis process, which reconverted into solids after cooling down. By combining with the HEA host, insulating sulfur blocks were divided into tiny particles, with conductive and catalytic HEA networks formed inside them.

The EDS analysis of the active substance in Fig. S2b shows that S, O, and corresponding metallic elements were detected on the surface of the sulfur/MgCrMnFeCoNi-O composite. It also indicates that the sulfur was successfully incorporated with the HEA host.

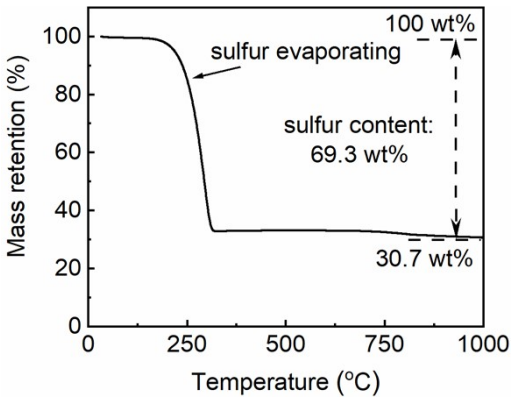

Fig. S3. The TGA curve for the sulfur-loaded MgCrMnFeCoNi-O nanoparticles.

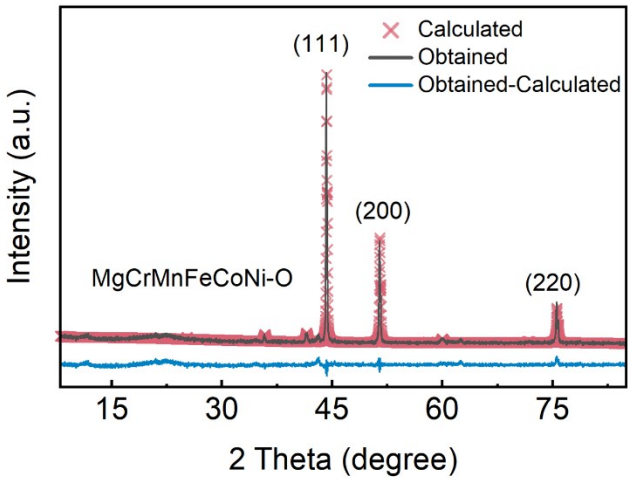

Fig. S4. The refined XRD pattern of pristine MgCrMnFeCoNi nanoparticles

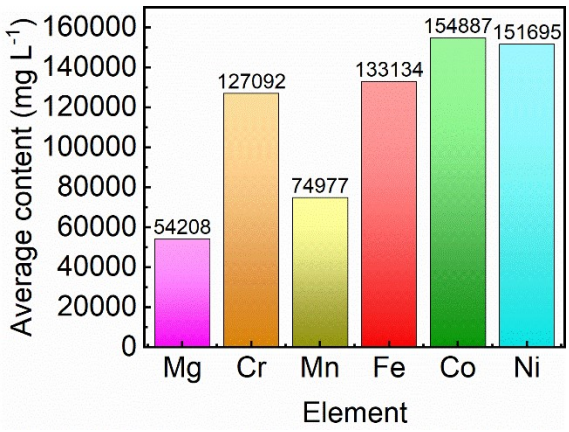

Fig. S5. ICP-OES result of the MgCrMnFeCoNi-O nanoparticle sample.

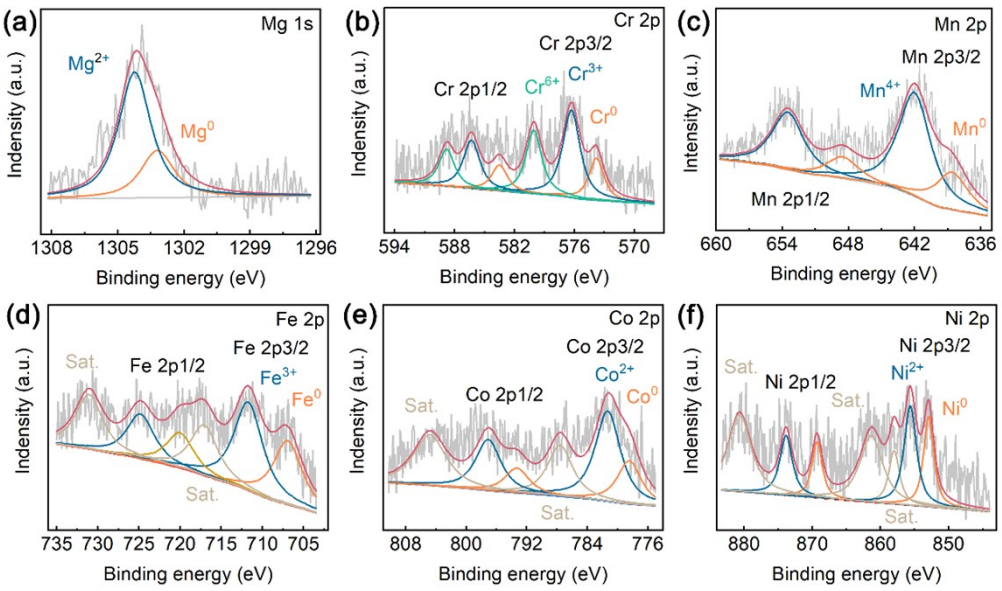

Fig. S6. XPS spectra of the MgCrMnFeCoNi-O nanoparticles: (a) Mg 1s, (b) Cr 2p, (c) Mn 2p, (d) Fe 2p, (e) Co 2p, and (d) Ni 2p spectra.

XPS spectra confirmed the coexistence of elemental state M^0 (M = Mg, Cr, Mn, Fe, Co, and Ni) and oxidation states (M^{x+}) on the surface of the MgCrMnFeCoNi-O nanoparticles. The Mg 1s narrow scan (Figure S3a) showed two peaks at the binding energy of 1303.2 eV and 1304.2 eV, which can be ascribed to Mg^0 and Mg^{2+}, respectively. In the spectrum of Cr 2p (Figure S3b), the peak at 573.8 eV is attributed to Cr^0, and those located at 576.3 eV and 580.0 eV can be attributable to Cr^{3+} and Cr^{6+}, respectively[1, 2]. The Mn 2p spectrum in Figure S3c shows two 3/2p peaks at 638.6 eV and 642.0 eV, corresponding to the signals of Mn^0 and Mn^{4+}, respectively[3]. Fe^0 and Fe^{3+} can be identified in the Fe 2p spectra (Figure S3d) at the binding energies of 706.9 eV and 711.7 eV, respectively[4]. In addition, the Co 2p3/2 peaks at 778.5 eV and 781.3 eV in Figure 3e are severally derived from Co^0 and Co^{2+}[5]. For the Ni 2p in Figure S3f, Ni^0 and Ni^{2+} can be confirmed by the Ni 2p3/2 peaks at 852.9 eV and 855.6 eV, respectively[6, 7].

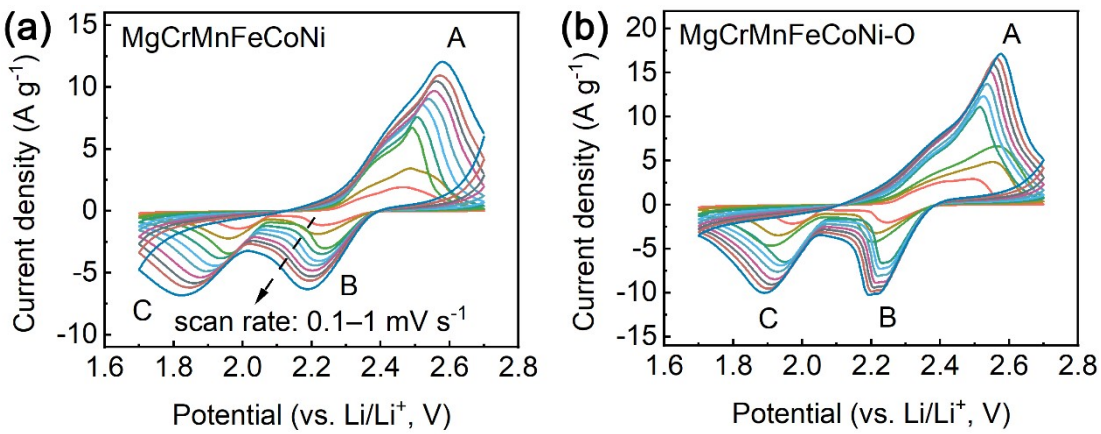

Fig. S7. CV profiles of (a) the MgCrMnFeCoNi and (b) MgCrMnFeCoNi-O electrodes obtained at various scan rates from 0.1 to 1 mV s^{-1}.

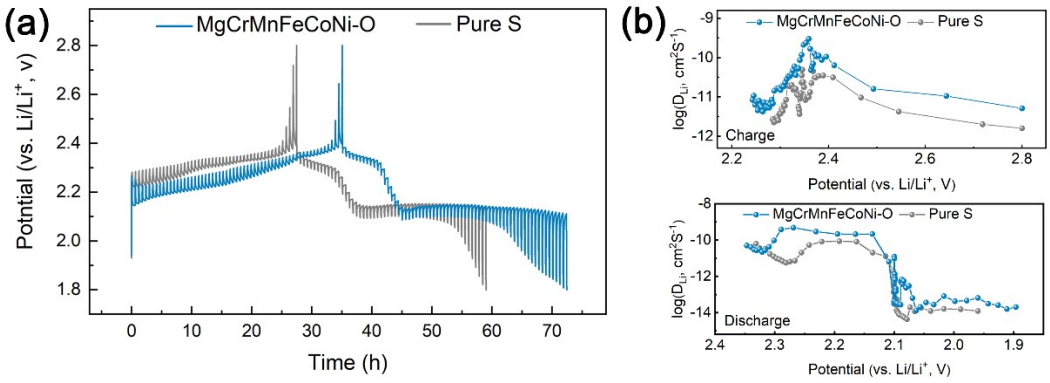

Fig. S8. GITT test of Li-S batteries with or without MgCrMnFeCoNi-O sulfur host: (a) the GITT curves; (b) corresponding values of Li^+ diffusivity (D_{Li}) in the charging process and discharging process

According to Fick's second law, the Li-ion diffusion coefficient can be calculated via the following equation

$$D_{Li} = \frac{4}{\pi\tau}\left(\frac{mV_m}{SM}\right)^2\left[\frac{\Delta E_s}{\Delta E_t}\right]^2, t \ll {L^2}/{D_{Li}}$$

where τ is the applied current period, m is the mass of the electrode material, M is the corresponding molar mass, ΔE_s is the steady-state potential change after a relaxation and charging/discharging process, and ΔE_t is the potential change caused by the constant current in the excitation time τ. The Li^+ diffusion coefficients of the pure S and MgCrMnFeCoNi-O cathode in the charging/discharging process are displayed in Fig. S8b above, which can be obtained from this equation. The resultant Li^+ diffusion coefficient of the MgCrMnFeCoNi-O cathode was within the range of 10^{-12} to 10^{-9} cm^2 S^{-1} in the charging process and 10^{-14} to 10^{-9} cm^2 S^{-1} in the discharging process, which is notably larger than that of the pure sulfur cathode. Based on the results, we consider that the Li^+ diffusivity in the cell can be promoted effectively when using MgCrMnFeCoNi-O nanoparticles as a sulfur host.

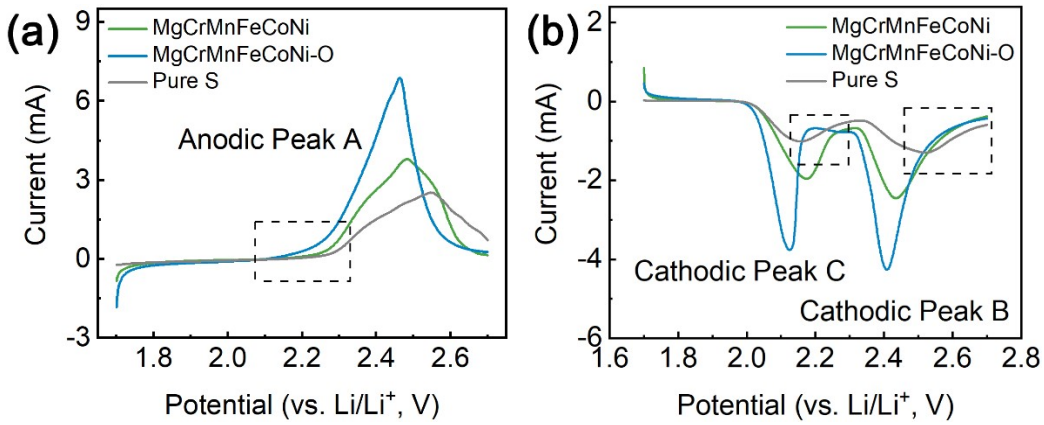

Fig. S9. LSV curves of the pure S, MgCrMnFeCoNi, and MgCrMnFeCoNi-O electrodes for (a) the anodic peak and (b) cathodic peaks at the scan rate of 0.2 mV s^{-1}.

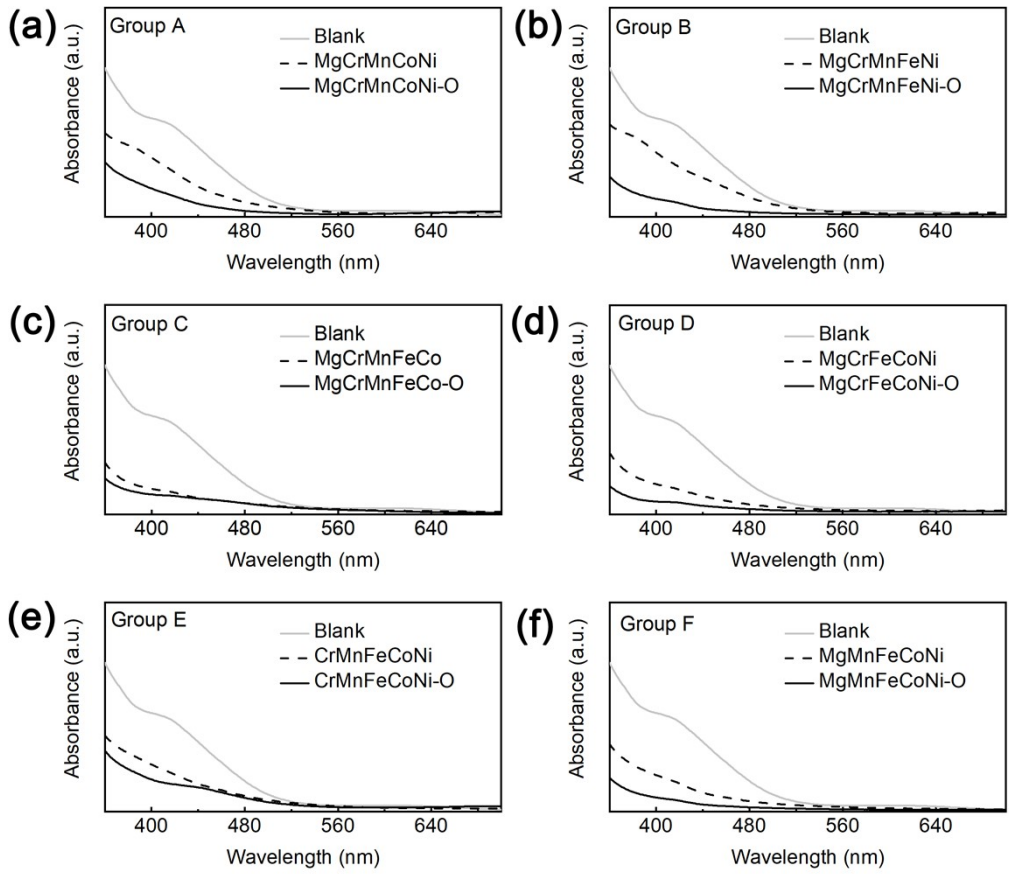

Fig. S10. UV–vis absorption spectra of the five-element HEA and corresponding oxidized HEA samples.

Sample number and the corresponding sample

Sample number	sample
A1	MgCrMnCoNi
A2	MgCrMnCoNi-O
B1	MgCrMnFeNi
B2	MgCrMnFeNi-O
C1	MgCrMnFeCo
C2	MgCrMnFeCo-O
D1	MgCrFeCoNi
D2	MgCrFeCoNi-O
E1	CrMnFeCoNi
E2	CrMnFeCoNi-O
F1	MgMnFeCoNi
F2	MgMnFeCoNi-O

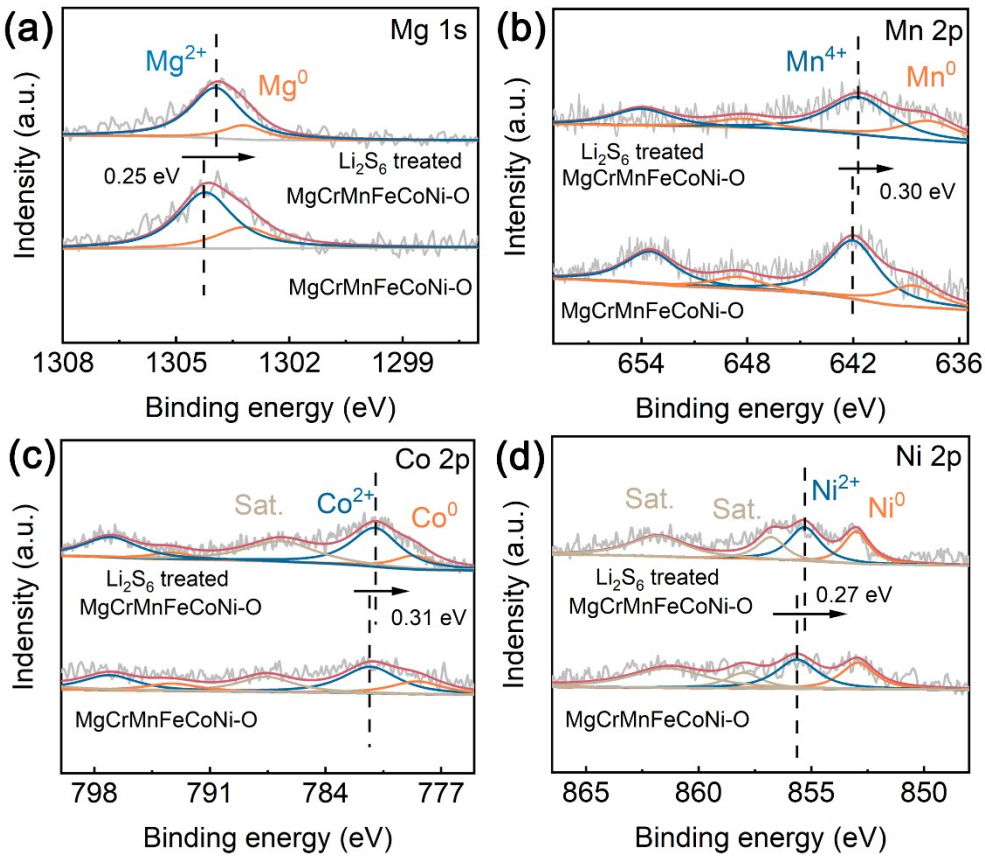

Fig. S11. XPS spectra of (a) Mg 1s, (b) Mn 2p, (c) Co 2p, and (d) Ni 2p of MgCrMnFeCoNi-O nanoparticles before and after absorbing Li_2S_6.

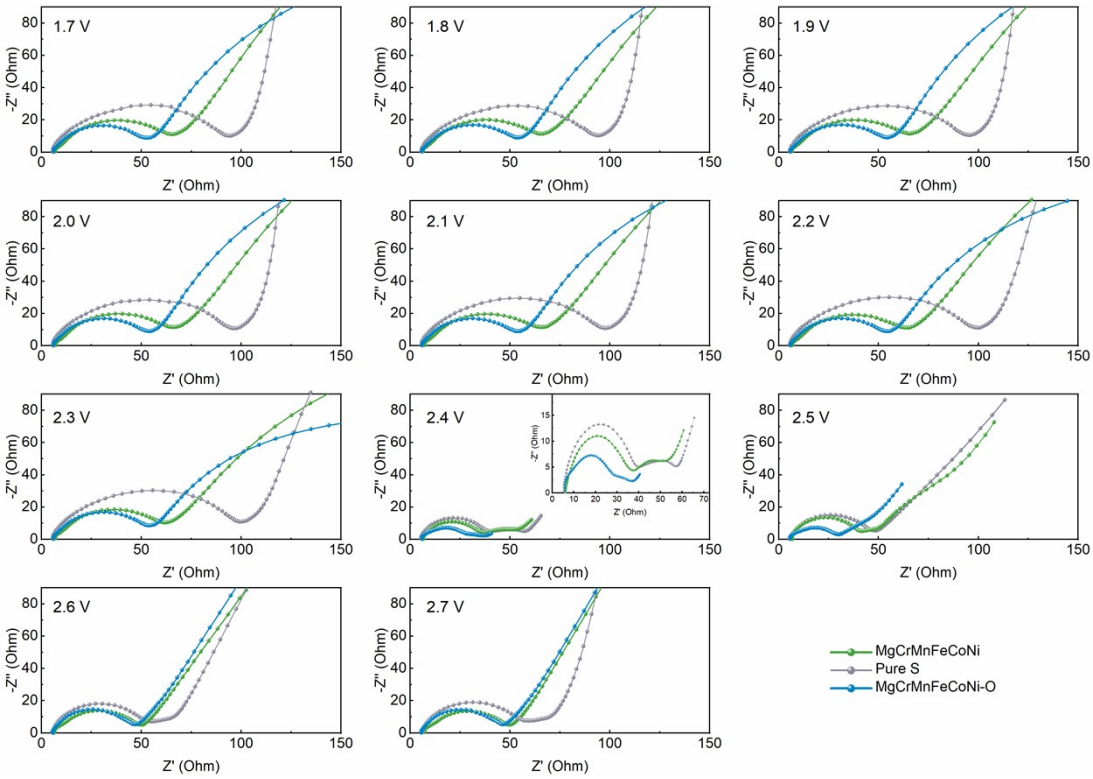

Fig. S12. Nyquist plots for the cells with pure S, MgCrMnFeCoNi, and MgCrMnFeCoNi-O cathodes at different potentials from 1.7 V to 2.7 V.

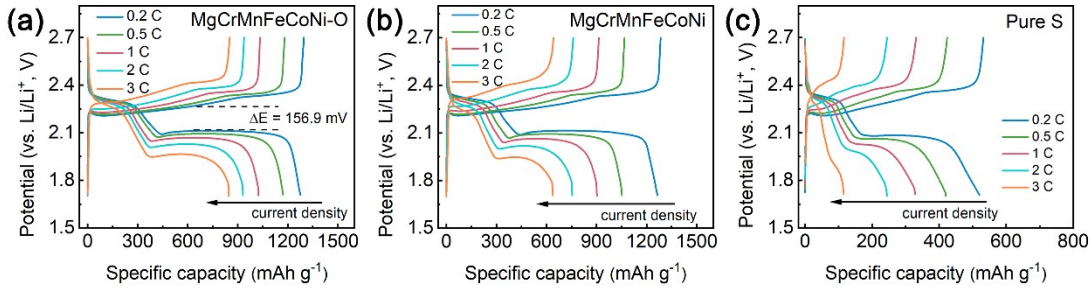

Fig. S13. Galvanostatic charge/discharge profiles of (a) the MgCrMnFeCoNi-O, (b) MgCrMnFeCoNi, and (c) pure S cathodes at various current densities from 0.2 C to 3 C.

References

1. Q. Yuan, L. Chen, M. Xiong, J. He, S.-L. Luo, C.-T. Au and S.-F. Yin, *Chem. Eng. J.*, 2014, **255**, 394-402.
2. X. Li, X. Gao, L. Ai and J. Jiang, *Chem. Eng. J.*, 2015, **274**, 238-246.
3. Y. Jin, L. Zou, L. Liu, M. H. Engelhard, R. L. Patel, Z. Nie, K. S. Han, Y. Shao, C. Wang, J. Zhu, H. Pan and J. Liu, *Adv. Mater.*, 2019, **31**, 1900567.
4. H. Zhang, C. Lin, X. Hu, B. Zhu and D. Yu, *ACS Appl. Mater. Interfaces*, 2018, **10**, 12708-12715.
5. X. Lv, Z. Xiao, H. Wang, X. Wang, L. Shan, F. Wang, C. Wei, X. Tang and Y. Chen, *J. Energy Chem.*, 2021, **54**, 626-638.
6. H. W. Nesbitt, D. Legrand and G. M. Bancroft, *Phys. Chem. Miner.*, 2000, **27**, 357-366.
7. B. Sarma, R. S. Ray, S. K. Mohanty and M. Misra, *Appl. Surf. Sci.*, 2014, **300**, 29-36.